



# Nonlinear forced vibration analysis of the composite shaft-disk system combined the reduced-order model with the IHB method

Kwangchol Ri · Wonjin Han · Choljun Pak · Kumchol Kim · Cholil Yun

Received: 31 October 2020 / Accepted: 30 April 2021 / Published online: 22 May 2021  
© The Author(s), under exclusive licence to Springer Nature B.V. 2021

**Abstract** In this paper, the internal resonance phenomena of a composite shaft-disk system with multi-degrees-of-freedom are analyzed. The force caused by the unbalanced mass of the disk is considered as an external excitation force. The shaft is simply supported. Shear deformation and gyroscopic effects are considered. The strain–displacement relationship of the shaft element is expressed using the Timoshenko beam theory. Each node has 5 degrees of freedom.

SHBT (simplified homogenized beam theory) is applied to calculate the stiffness of the composite shaft. WQEM (weak form quadrature element method) is used to construct the element matrices, and the system matrices are established using the element matrix assembly rule of the FEM (finite element method). The reduced-order model is applied to reduce the calculation time. IHB (incremental harmonic balance) method is utilized to solve the nonlinear equations of motion of the composite shaft-disk system. The nonlinear vibration characteristics of the Jeffcott rotor are analyzed using the proposed method and compared with the results of previous researches, and the results are very similar. Based on these considerations, the nonlinear vibration phenomena of the composite shaft-disk system with multi-degrees-of-freedom are considered at the several resonance points.

---

K. Ri (✉)  
Department of Light Industry Machinery Engineering,  
Pyongyang University of Mechanical Engineering,  
Pyongyang 999093, Democratic People’s Republic of  
Korea

W. Han  
Faculty of Life Sciences, Pyongyang University of  
Science and Technology, Pyongyang 999093, Democratic  
People’s Republic of Korea

C. Pak  
College of Ship and Ocean Technology, Kim Chaek  
University of Technology, Pyongyang 999093,  
Democratic People’s Republic of Korea

K. Kim  
Faculty of Physical Engineering, Kim Chaek University  
of Technology, Pyongyang 999093, Democratic People’s  
Republic of Korea

C. Yun  
Faculty of Forest Science, Kim Il Sung University,  
Pyongyang 999093, Democratic People’s Republic of  
Korea

**Keywords** Composite shaft · Nonlinear vibration · Rotor dynamics · Reduced-order model · IHB

## 1 Introduction

Composite materials have the high ratio of strength to density, high ratio of stiffness to density, high fatigue strength. So, it is widely used in many industries such as automobile, shipbuilding, and aerospace. In particular, the composite shaft has the characteristics of low

noise, low energy consumption, high speed and stable control, and is widely used in automobiles, helicopters and other mechanical equipment. At present, the rotating machines operate beyond the critical speed, and when they pass through the critical speed, vibration with large amplitude occurs [1]. Therefore, it is of practical significance to accurately analyze the dynamic characteristics of the composite shaft and ensure its stable operation.

Many researchers have proposed many different models to analyze the dynamic characteristics of the composite shaft. Singh et al. [2] used EMBT (equivalent modulus beam theory) to calculate the equivalent longitudinal and in-plane shear moduli of the composite shaft and calculated its natural frequency by using the calculation method for the isotropic materials shaft. Gubran et al. [3] overcame the shortcomings of EMBT and proposed the modified EMBT, which improved the calculation accuracy by considering various coupling effects in composite materials. Sino et al. [4] used SHBT to calculate the stiffness of the composite shaft and proposed a homogenized finite element beam model considering the internal damping. On this basis, they calculated its natural frequency and instability thresholds. Ri et al. [5] added the coupling effects of composite materials to SHBT and improved the calculation accuracy. Singh et al. [6] applied LBT theory, which provided a more real strain field, to calculate the natural frequency of the composite shaft. However, LBT provides a more accurate deformation representation than other theories, and it consumes a lot of computation time when the number of the layer increases. As all the theories mentioned above are considering the linear vibration model of the composite shaft, it is only possible to calculate the basic values such as natural frequency and instability threshold.

Many different models have been proposed to analyze the nonlinear vibration of rotating shaft system. Ishida et al. [7] analyzed the nonlinear forced vibration of vertical continuous rotor with distribution mass. They studied the possibility of nonlinear forced vibration at various subcritical speeds. Ishida et al. [8] studied the internal resonance phenomena of Jeffcott rotor having a nonlinear spring characteristics. They concluded that if Jeffcott rotor was used in the analysis of rotor system, the result was not correct. Ishida et al. [9] considered the unstable vibration phenomena of asymmetrical rotating shaft. They studied the internal

resonance phenomena of the shaft in the vicinity of the major critical speed and the rotational speed vicinity of twice and three times the major critical speed. Inoue et al. [10] investigated the chaotic vibration caused by 1 to (-1) type internal resonance in the vicinity of the major critical speed and the rotational speed, which is twice the major critical speed. Khadem et al. [11] analyzed the primary resonances of a simply supported in-extensional rotating shaft, where the multiple scales method was applied to analyze the nonlinear vibration. Hosseini et al. [12] analyzed the free vibration of rotating shaft with stretching nonlinearity using the multiple scales method. They also studied the vibration characteristics of spinning beam with geometrical nonlinearity [13]. Zhang et al. [14] applied IHB method to analyze the nonlinear vibration of the composite shaft-disk rotating system considering nonlinear deformation. In this paper, frequency–response characteristics according to the change of several parameters were studied. Nezhad et al. [15] applied the harmonic balance method to analyze the nonlinear vibration characteristics of the composite shaft. Shaban et al. [16] analyzed flexural–flexural–extensional–torsional vibration of the composite shaft considering the geometrical nonlinearity by method of multiple scales.

Due to imbalance caused by manufacturing errors, shaft mismatches, and bearing wear mismatches, nonlinear vibration occurs in the rotating shaft [17]. The nonlinear vibration characteristics of the composite shaft-disk system caused by unbalanced mass have been analyzed by many researchers. However, little research has been done on the internal resonance phenomena occurring in these systems.

To solve the nonlinear vibration equation, the perturbation method and HBM (harmonic balance method) are used. The perturbation method is used for analyzing the weak nonlinear systems. Fourier series is applied for the time solution in HBM and it has the advantage of being used in both weak nonlinear systems and strong nonlinear systems. The disadvantage of HBM is to consume lots of computation time. As the number of harmonic terms and degree of freedom increases, the order of the matrix increases, which consumes more computation time. Because IHB method combines Newton–Raphson method and HBM, it has a same shortcoming. To overcome this shortcoming, the reduced-order model is used in this article. Until now, the research on the analysis of

nonlinear vibration of rotor system using reduced-order model and IHB method has not been widely conducted.

This paper provided the solution method for the analysis of nonlinear vibration of the composite shaft-disk system with multi-degree-of-freedom which combines the reduced-order model with IHB method. Employing the proposed method, the internal resonance phenomena of the composite shaft-disk system occurring at the several resonance points are analyzed. SHBT is used to calculate the stiffness of the composite shaft. Timoshenko beam theory is used for the strain–displacement relationship, and the kinetic and strain energies of element are expressed using WQEM. The element equations of motion is established by using Lagrange’s equation, and the equations of the whole system are established by using element matrix assembly method in FEM. The reduced-order model of shaft-disk system is established using modal matrix composing of modal coordinates and eigenvectors of linear eigenvalue equations. The number of modes used in the reduced-order model is determined by analyzing the nonlinear vibration characteristics using the reduced-order model and non-reduced order models and comparing the results. Though the IHB method is applied to solve the nonlinear equation, using the IHB method alone, it is impossible to obtain complex frequency–response characteristics near the resonance point. The response at frequencies far from the resonance point is calculated using only the IHB method. However, the frequency response near the resonance point is calculated by the continuation technique. To prove the validity of the proposed model, the nonlinear vibration characteristics of the Jeffcott rotor are calculated by the proposed method. The analysis results and the results of the reference [23] are very close. Based on these results, in this paper, the shaft-disk system is expanded to a model with multi-degree of freedom, and the internal resonance phenomena of the composite shaft-disk system are studied at several resonance points.

## 2 Weak form quadrature element method

WQEM is similar with higher-order FEM and more flexible than strong form quadrature element method, therefore it is widely applied in the analysis of

engineering problems. Using WQEM, the element matrices of shaft element are calculated. Gauss–Lobatto–Legendre points are used as nodal points of shaft element. Gauss–Lobatto–Legendre points are the solution of Eq. (1).

$$(1 - x^2) \frac{dP_{n-1}(x)}{dx} = 0 \tag{1}$$

Here,  $x$  is defined at  $[-1, 1]$  and  $P_{n-1}(x)$  is  $(n - 1)$ th Legendre polynomial.

The function  $f(x)$  defined at  $[-1, 1]$  is integrated using Gauss–Lobatto–Legendre quadrature rule as follows [18].

$$\int_{-1}^1 f(x)dx = \sum_{j=1}^n C_j f(x_j) \tag{2}$$

Here,  $C_j$  is the weighting coefficient calculated by Gauss–Lobatto–Legendre quadrature rule.  $n$  is the number of nodal points. The weighting coefficient is calculated as follows.

$$C_1 = C_n = \frac{2}{n(n-1)},$$

$$C_j = \frac{2}{n(n-1)[P_{n-1}(x_j)]^2} (j \neq 1, n) \tag{3}$$

The  $m$ -order derivative of function  $f$  is approximated as follows [18].

$$f_i^{(m)} = \sum_{j=1}^n A_{ij}^{(m)} f_j (i = 1, 2 \dots, N) \tag{4}$$

Here,  $A_{ij}^{(m)}$  is  $m$ -order weighting coefficient. Because Timoshenko beam theory is applied in this research, only the first-order derivative is used in the strain expression. Therefore, only the first-order weighting coefficient matrix is considered. The elements on the diagonal and outside of diagonal of the first-order weighting coefficient matrix are given in Eqs. (5) and (6).

$$A_{ii}^{(1)} = - \sum_{j=1, j \neq i}^n A_{ij}^{(1)} \tag{5}$$

$$A_{ij}^{(1)} = \frac{\prod_{k=1, k \neq i}^n (x_i - x_k)}{(x_i - x_j) \prod_{k=1, k \neq j}^n (x_j - x_k)} \tag{6}$$

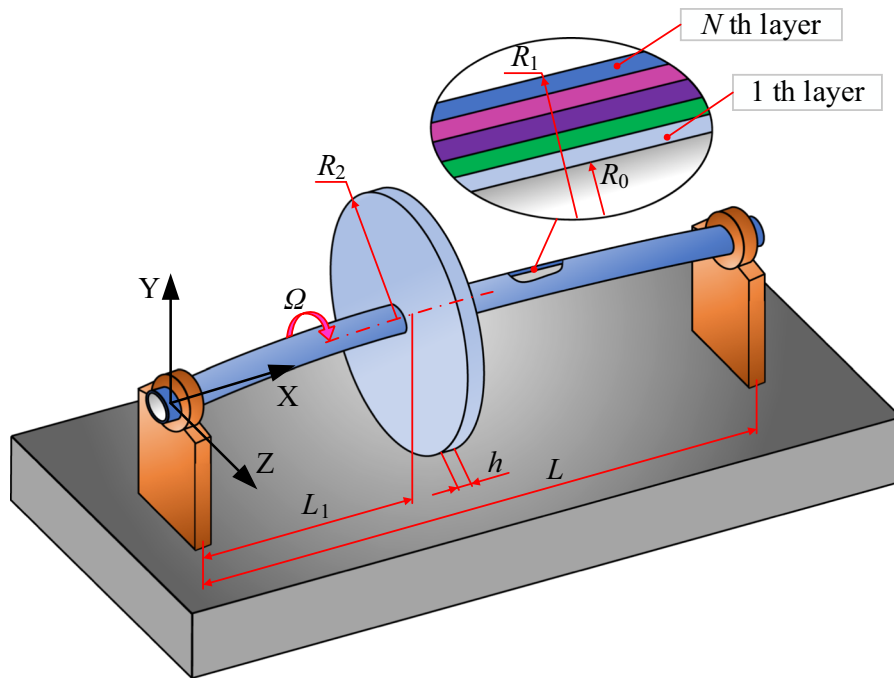


**Fig. 1** Coordinate system of the composite shaft-disk system

The nodal points introduced in Eqs. (2) and (4) have same distribution forms, that is, defined at  $[-1, 1]$ . However, in practice, nodal points are not placed in the interval  $[-1, 1]$ , so the formula above should be changed as follows.

$$\mathbf{A}^{(1)} = \frac{2}{l_e} \mathbf{A}_{01}^{(1)}, \quad \mathbf{C}^{(1)} = \frac{l_e}{2} \mathbf{C}_{01}^{(1)} \tag{7}$$

Here,  $\mathbf{A}_{01}^{(1)}$  and  $\mathbf{C}_{01}^{(1)}$  are the first-order weighting coefficient matrices defined at  $[-1, 1]$ .

### 3 Motion equation

Using Timoshenko beam theory, the composite shaft is modeled as a beam element and the disk as a rigid element. Figure 1 shows the coordinate system and geometrical dimension of the composite shaft-disk system. The composite shaft is composed of laminate structures with different fiber angles. The cross section is circular and rotates around X-axis.

Figure 2 shows the displacement of shaft element and layer allocation of the composite shaft considered in this research.

The strains on the shaft element are defined as follows using the von Karman’s theory [19].

$$\varepsilon_{xx} = \varepsilon_{xx}^0 + zk_{yy}^0 + yk_{zz}^0, \quad \gamma_{xy} = \gamma_{xy}^0, \quad \gamma_{xz} = \gamma_{xz}^0 \tag{8}$$

$$\begin{aligned} \varepsilon_{xx}^0 &= \frac{\partial u}{\partial x} + \frac{1}{2} \left( \frac{\partial v}{\partial x} \right)^2 + \frac{1}{2} \left( \frac{\partial w}{\partial x} \right)^2, & k_{yy}^0 &= \frac{\partial \beta}{\partial x}, \\ k_{zz}^0 &= \frac{\partial \gamma}{\partial x}, & \gamma_{xy}^0 &= \frac{\partial v}{\partial x} - \gamma, & \gamma_{xz}^0 &= \frac{\partial w}{\partial x} + \beta \end{aligned} \tag{9}$$

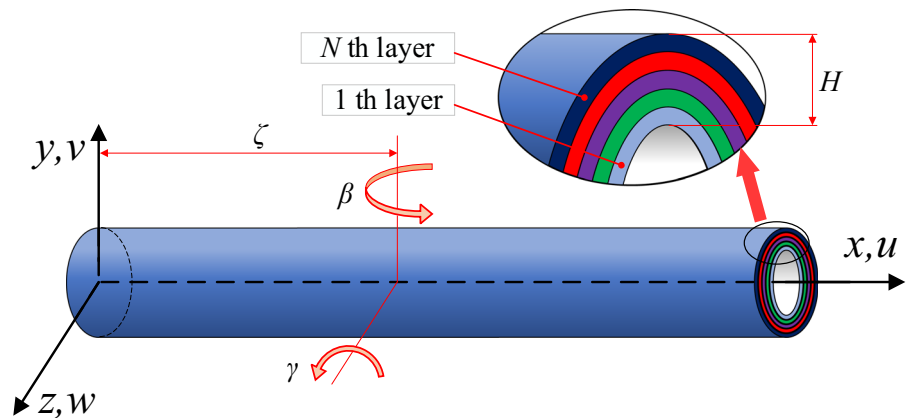
Here  $u, v$  and  $w$  mean the displacements of any points on the middle surface of the shaft element in the  $x, y,$  and  $z$  directions, respectively.  $\beta$  and  $\gamma$  indicate the rotations of any cross sections around the  $y$  and  $z$  axes, respectively.

The composite shaft-disk system has kinetic energy due to disk, shaft and unbalanced mass, and strain energy on the shaft. The kinetic energy of the disk is as follows [5].

$$\begin{aligned} T_d^e &= \frac{1}{2} \sum_{i=1}^{nd} \left[ M_{di} \left( \dot{u}(x_i)^2 + \dot{v}(x_i)^2 + \dot{w}(x_i)^2 \right) \right. \\ &\quad \left. + I_{di} \left( \dot{\beta}(x_i)^2 + \dot{\gamma}(x_i)^2 \right) + I_{dpi} \Omega \dot{\beta}(x_i) \gamma(x_i) \right] \end{aligned} \tag{10}$$

Here,  $x_i$  is the position of disk on the shaft,  $nd$  is the number of disks, and  $\Omega$  is the rotating angular speed of

**Fig. 2** The displacements of shaft elements and layer allocation of the composite shaft



the shaft.  $M_{di}$  denotes the mass of the  $i$ -th disk, and  $I_{di}$  and  $I_{dpi}$  depict the lateral and polar area moments of inertia of shaft cross section of the  $i$ -th disk.

The kinetic energy of the shaft is as follows [5].

$$T_s^e = \frac{1}{2} \int_0^{l_e} [I_0(\dot{u}^2 + \dot{v}^2 + \dot{w}^2) + I_1(\dot{\beta}^2 + \dot{\gamma}^2) + 2I_2\Omega\dot{\beta}\dot{\gamma}] dx \tag{11}$$

Here,  $l_e$  indicates the length of elements. In this formula,  $I_0 = \rho_s S$ ,  $I_1 = \rho_s I$  and  $I_2 = \rho_s I_p$ .  $\rho_s$  is the density of the shaft.

$S$  indicates area of the shaft cross-section, and  $I$  and  $I_p$  represent the lateral and polar area moments of inertia of shaft cross section, respectively.

The kinetic energy due to the unbalanced mass of disk is expressed as follows [11].

$$T_u^e = \sum_{i=1}^{nd} M_{di} \Omega \{ \dot{v} [e_{\xi i} \sin \Omega t + e_{\zeta i} \cos \Omega t] + \dot{w} [-e_{\xi i} \cos \Omega t + e_{\zeta i} \sin \Omega t] \} + \frac{1}{2} \sum_{i=1}^{nd} M_{di} \Omega^2 [e_{\xi i}^2 + e_{\zeta i}^2] \tag{12}$$

Here,  $e_{\xi}$  and  $e_{\zeta}$  are the eccentricity distribution measured in the coordinate fixed on the disk.

The strain energy of the shaft is as follows [5].

$$U^e = \frac{1}{2} \int_0^{l_e} [E_{eqs} e_{xx}^2 + E_{eq} (k_{yy}^2 + k_{zz}^2) + G_{eq} (\gamma_{xy}^2 + \gamma_{xz}^2)] dx \tag{13}$$

$$E_{eqs} = \pi \sum_{k=1}^N E_{eq}^k (R_{o(k)}^2 - R_{i(k)}^2) \tag{14}$$

$$E_{eq} = \frac{\pi}{4} \sum_{k=1}^N E_{eq}^k (R_{o(k)}^4 - R_{i(k)}^4) \tag{15}$$

$$G_{eq} = k' \sum_{k=1}^N G_{eq}^k S^k \tag{16}$$

Here  $k'$  is the shear correction factor.  $R_{o(k)}$ ,  $R_{i(k)}$  represent the inner and outer radii of the  $k$ -th layer.

In Eqs. (15) and (16),  $E_{eq}^k$ ,  $G_{eq}^k$  are calculated as follows [5].

$$E_{eq}^k = \frac{1}{\frac{1}{E_1^k} \cos^4 \theta_k + \left( \frac{1}{G_{12}^k} - \frac{2\nu_{12}^k}{E_1^k} \right) \sin^2 \theta_k \cos^2 \theta_k + \frac{1}{E_2^k} \sin^4 \theta_k} \tag{17}$$

$$G_{eq}^k = \frac{1}{4 \cos^2(\theta_k) \sin^2(\theta_k) \left( \frac{1}{E_1^k} + \frac{1}{E_2^k} + 2 \frac{\nu_{21}^k}{E_1^k} \right) + \frac{(\cos^2(\theta_k) - \sin^2(\theta_k))^2}{G_{12}^k}} \tag{18}$$

Here,  $\theta_k$  represents the lamination angle of the  $k$ -th layer.  $E_1^k$ ,  $G_{12}^k$ , and  $\nu_{12}^k$  are engineering constants of the  $k$ -th layer.

The strain energy of shaft is composed of linear strain energy and nonlinear strain energy, and these energies are as follows.

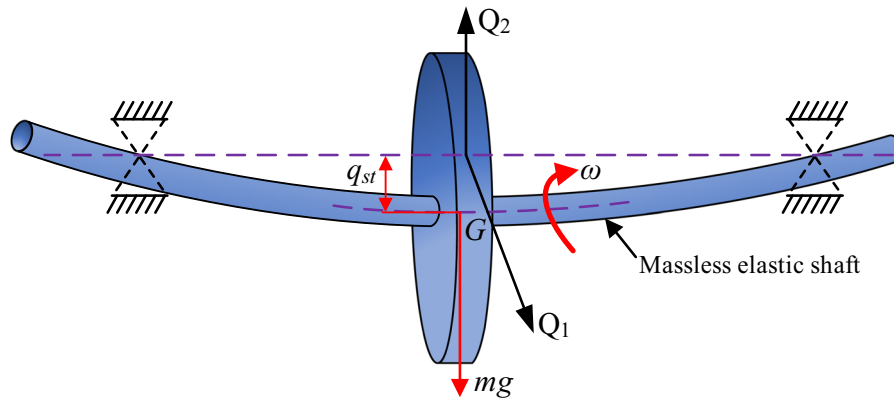


Fig. 3 Jeffcott rotor system

$$U_L^e = \frac{1}{2} \int_0^{l_e} \left\{ E_{eqs} \left( \frac{\partial u}{\partial x} \right)^2 + E_{eq} \left[ \left( \frac{\partial \beta}{\partial x} \right)^2 + \left( \frac{\partial \gamma}{\partial x} \right)^2 \right] + G_{eq} \left[ \left( \frac{\partial v}{\partial x} - \gamma \right)^2 + \left( \frac{\partial w}{\partial x} + \beta \right)^2 \right] \right\} dx \tag{19}$$

$$U_{NL}^e = \frac{E_{eqs}}{2} \int_0^{l_e} \left[ \frac{1}{4} \left( \frac{\partial v}{\partial x} \right)^4 + \frac{1}{4} \left( \frac{\partial w}{\partial x} \right)^4 + \frac{\partial u}{\partial x} \left( \frac{\partial v}{\partial x} \right)^2 + \frac{\partial u}{\partial x} \left( \frac{\partial w}{\partial x} \right)^2 + \frac{1}{2} \left( \frac{\partial v}{\partial x} \right)^2 \left( \frac{\partial w}{\partial x} \right)^2 \right] dx \tag{20}$$

The displacements and rotations of cross section are expressed as follows using the method of separation of variables.

$$\begin{aligned} u(x, t) &= U(x) \cdot q_u(t) \\ v(x, t) &= V(x) \cdot q_v(t) \\ w(x, t) &= W(x) \cdot q_w(t) \\ \beta(x, t) &= B(x) \cdot q_\beta(t) \\ \gamma(x, t) &= \Gamma(x) \cdot q_\gamma(t) \end{aligned} \tag{21}$$

To simplify the calculation, the non-dimensional variables as follows are introduced.

$$\begin{aligned} \xi &= \frac{x}{l_e}, R = \sqrt{\frac{I}{S}}, H = \rho_{d1} S_1 \\ \tilde{u} &= \frac{U}{R}, \tilde{v} = \frac{V}{R}, \tilde{w} = \frac{W}{R}, \tilde{\beta} = \frac{l_e}{R} B, \tilde{\gamma} = \frac{l_e}{R} \Gamma \\ \tilde{t} &= t \omega_0, \tilde{\Omega} = \frac{\Omega}{\omega_0}, \psi = \frac{R}{l_e}, \tilde{I}_0 = \frac{I_0}{H}, \tilde{I}_1 = \frac{I_1}{H l_e^2}, \tilde{I}_2 = \frac{I_2}{H l_e^2} \\ \tilde{M}_{di} &= \frac{M_{di}}{H l_e}, \tilde{I}_{di} = \frac{I_{di}}{H l_e^3}, \tilde{I}_{dpi} = \frac{I_{dpi}}{H l_e^3}, \tilde{e}_{\xi i} = \frac{e_{\xi i}}{R}, \tilde{e}_{\zeta i} = \frac{e_{\zeta i}}{R} \\ E_{eqs} &= \frac{E_{eqs}}{\omega_0^2 H l_e^2}, \tilde{E}_{eq} = \frac{E_{eq}}{\omega_0^2 H l_e^4}, \tilde{G}_{eq} = \frac{G_{eq}}{\omega_0^2 H l_e^2} \end{aligned} \tag{22}$$

Here,  $I = \frac{\pi(R_2^4 - R_1^4)}{4}$ ,  $S = \pi(R_2^2 - R_1^2)$ .  $R_1$  and  $R_2$  are the inner and outer radii of the disk.  $\rho_{d1}$  and  $S_1$  are the density and area of the first disk.  $\omega_0$  is the first natural frequency of the composite shaft-disk system in the non-rotating state.  $M_{di}$ ,  $I_{di}$ , and  $I_{dpi}$  are defined as follows [20].

$$M_{di} = \pi(R_{2i}^2 - R_{1i}^2) h_i \rho_{di} \tag{23}$$

$$I_{di} = \frac{M_{di}}{12} (3R_{1i}^2 + 3R_{2i}^2 + h_i^2) \tag{24}$$

$$I_{dpi} = \frac{M_{di}}{2} (R_{1i}^2 + R_{2i}^2) \tag{25}$$

Here  $\rho_{di}$  is the density of the  $i$ -th disk.  $R_{1i}$  and  $R_{2i}$  are the inner and outer radii of the  $i$ -th disk.  $h_i$  is the thickness of the  $i$ -th disk.

The kinetic energy and strain energy are expressed with the non-dimensional variables as follows.

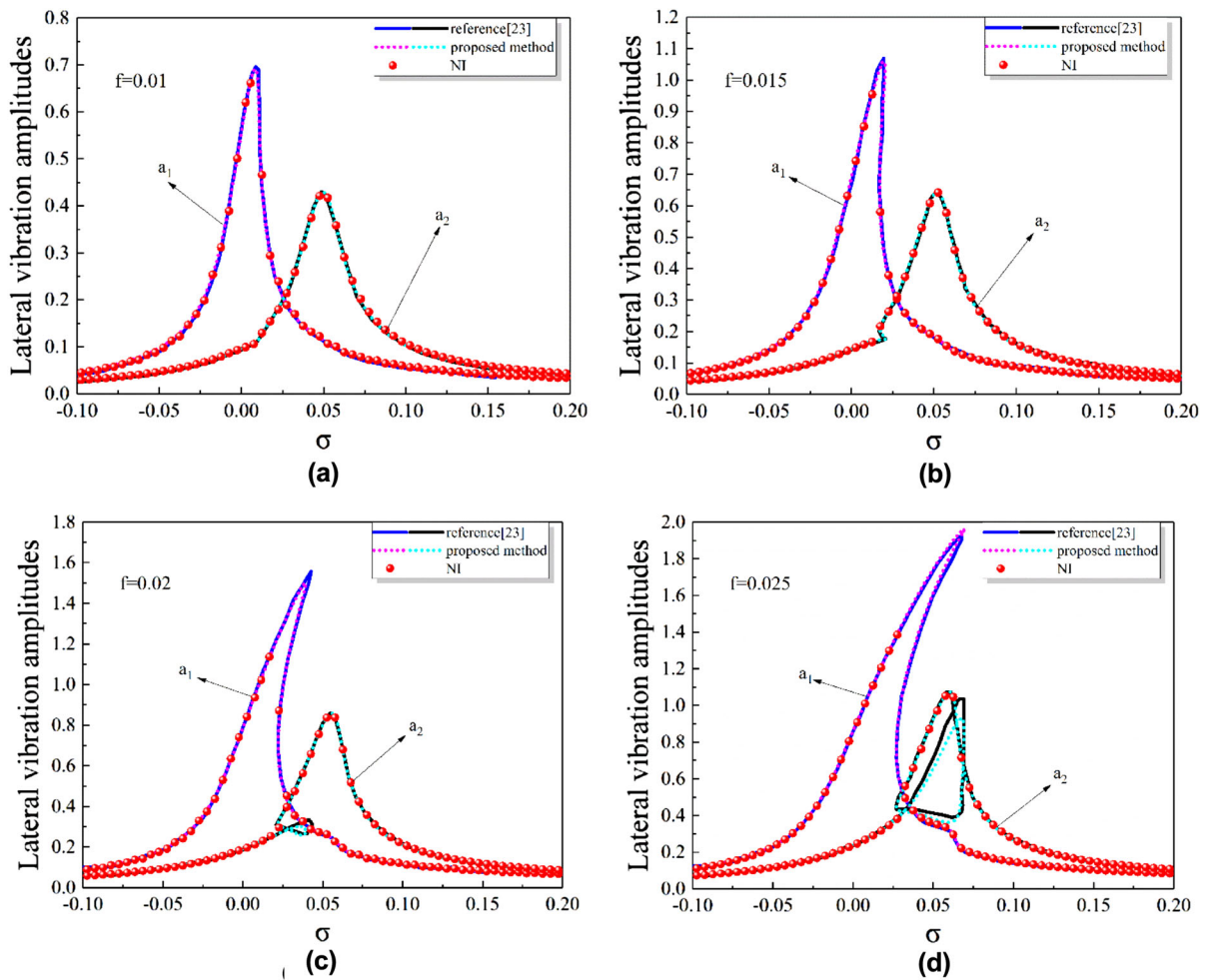


**Fig. 4** The comparison of the frequency–response curves of Jeffcott rotor calculated by the proposed method and multiple scales perturbation method

$$T_d^e = \frac{\omega_0^2 H l_e R^2}{2} \sum_{i=1}^{nd} \left[ \tilde{M}_{di} \left( \dot{\tilde{u}}(x_i)^2 + \dot{\tilde{v}}(x_i)^2 + \dot{\tilde{w}}(x_i)^2 \right) + \tilde{I}_{di} \left( \dot{\tilde{\beta}}(x_i)^2 + \dot{\tilde{\gamma}}(x_i)^2 \right) + 2\tilde{I}_{dpi} \tilde{\Omega} \dot{\tilde{\beta}}(x_i) \tilde{\gamma}(x_i) \right] \quad (26)$$

$$T_s^e = \frac{\omega_0^2 H l_e R^2}{2} \int_0^1 \left[ (\dot{\tilde{u}}^2 + \dot{\tilde{v}}^2 + \dot{\tilde{w}}^2) + \tilde{I}_1 (\dot{\tilde{\beta}}^2 + \dot{\tilde{\gamma}}^2) + 2\tilde{I}_2 \tilde{\Omega} \dot{\tilde{\beta}} \tilde{\gamma} \right] d\zeta \quad (27)$$

$$T_u^e = \omega_0^2 H l_e R^2 \sum_{i=1}^{nd} \tilde{M}_{di} \tilde{\Omega} \left\{ \dot{\tilde{v}} \left[ \tilde{e}_{\zeta i} \sin \tilde{\Omega} \tilde{t} + \tilde{e}_{\zeta i} \cos \tilde{\Omega} \tilde{t} \right] + \dot{\tilde{w}} \left[ -\tilde{e}_{\zeta i} \cos \tilde{\Omega} \tilde{t} + \tilde{e}_{\zeta i} \sin \tilde{\Omega} \tilde{t} \right] \right\} + \frac{\omega_0^2 H l_e R^2}{2} \sum_{i=1}^{nd} \tilde{M}_{di} \tilde{\Omega}^2 \left[ \tilde{e}_{\zeta i}^2 + \tilde{e}_{\zeta i}^2 \right] \quad (28)$$

$$U_L^e = \frac{\omega_0^2 H l_e R^2}{2} \int_0^1 \left\{ \tilde{E}_{eqs} \left( \frac{\partial \tilde{u}}{\partial \xi} \right)^2 + \tilde{E}_{eq} \left[ \left( \frac{\partial \tilde{\beta}}{\partial \xi} \right)^2 + \left( \frac{\partial \tilde{\gamma}}{\partial \xi} \right)^2 \right] + \tilde{G}_{eq} \left[ \left( \frac{\partial \tilde{v}}{\partial \xi} - \tilde{\gamma} \right)^2 + \left( \frac{\partial \tilde{w}}{\partial \xi} + \tilde{\beta} \right)^2 \right] \right\} d\xi \tag{29}$$

$$U_{NL}^e = \frac{\omega_0^2 H l_e R^2}{2} \int_0^1 \tilde{E}_{eqs} \left[ \frac{1}{4} \psi^2 \left( \frac{\partial \tilde{v}}{\partial \xi} \right)^4 + \frac{1}{4} \psi^2 \left( \frac{\partial \tilde{w}}{\partial \xi} \right)^4 + \psi \frac{\partial \tilde{u}}{\partial \xi} \left( \frac{\partial \tilde{v}}{\partial \xi} \right)^2 + \psi \frac{\partial \tilde{u}}{\partial \xi} \left( \frac{\partial \tilde{w}}{\partial \xi} \right)^2 + \frac{1}{2} \psi^2 \left( \frac{\partial \tilde{v}}{\partial \xi} \right)^2 \left( \frac{\partial \tilde{w}}{\partial \xi} \right)^2 \right] d\xi \tag{30}$$

The character ‘~’ indicates non-dimensional variables. Because the item  $\omega_0^2 H l_e R^2$  exists in all the energy equations, this item is deleted when the motion equation is established.

Using the WQEM and Lagrange’s equation, the motion equation of element is expressed as follows.

$$\mathbf{M}^e \ddot{\mathbf{q}}^e + \mathbf{G}^e \dot{\mathbf{q}}^e + (\mathbf{K}^e + \mathbf{K}_3^e) \mathbf{q}^e = \Omega^2 \mathbf{F}^e \tag{31}$$

Here,  $\mathbf{M}^e$  is the mass matrix,  $\mathbf{G}^e$  is the gyroscopic matrix,  $\mathbf{K}^e$  is the linear stiffness matrix,  $\mathbf{K}_3^e$  is the nonlinear stiffness matrix and  $\Omega^2 \mathbf{F}^e$  is the force matrix caused by unbalanced mass. The character ‘e’ indicates the element matrix. The expression of element matrix is given in appendix in detail. The total system matrix can be obtained by assembling the element matrixes according to the element matrix assembly rule of FEM. Using the total system matrix, the motion equation of the composite shaft-disk system is expressed as follows.

$$\mathbf{M} \ddot{\mathbf{q}} + \mathbf{G} \dot{\mathbf{q}} + (\mathbf{K} + \mathbf{K}_3) \mathbf{q} = \Omega^2 \mathbf{F} \tag{32}$$

The motion equation of the system includes the nonlinear term. To solve the nonlinear vibration equation, IHB method is applied in this research.

#### 4 Reduced-order model

When the vibration characteristics of the structure is analyzed using the FEM, many degree of freedom is used. To overcome these disadvantages, the reduced-order model is established.

First of all, using the mass matrix  $\mathbf{M}$  and linear stiffness matrix  $\mathbf{K}$  in Eq. (32), the linear free vibration equation is established as follows.

$$(-\omega_0^2 \mathbf{M} + \mathbf{K}) \mathbf{q} = \mathbf{0} \tag{33}$$

The modal matrix  $\Phi$  is obtained by solving this linear eigenvalue equation. Using this modal matrix and modal coordinate  $\mathbf{p}$ , vector  $\mathbf{q}$  can be expressed as follows.

$$\mathbf{q} = \Phi_s \mathbf{p} \tag{34}$$

Here,  $s$  is the number of modes used in the analysis. Equation (34) is substituted into Eq. (32).

$$\mathbf{M} \Phi_s \ddot{\mathbf{p}} + \mathbf{G} \Phi_s \dot{\mathbf{p}} + (\mathbf{K} + \mathbf{K}_3) \Phi_s \mathbf{p} = \Omega^2 \mathbf{F} \tag{35}$$

Multiply  $\Phi_s^T$  with the left part of Eq. (35) to get the following equation.

$$\mathbf{m} \ddot{\mathbf{p}} + \mathbf{g} \dot{\mathbf{p}} + (\mathbf{k} + \mathbf{k}_3) \mathbf{p} = \Omega^2 \mathbf{f} \tag{36}$$

Here,

$$\begin{aligned} \mathbf{m} &= \Phi_s^T \mathbf{M} \Phi_s \\ \mathbf{g} &= \Phi_s^T \mathbf{G} \Phi_s \\ \mathbf{k} &= \Phi_s^T \mathbf{K} \Phi_s \\ \mathbf{k}_3 &= \Phi_s^T \mathbf{K}_3 \Phi_s \\ \mathbf{f} &= \Phi_s^T \mathbf{F} \end{aligned} \tag{37}$$

#### 5 IHB Method

IHB method is used to solve the nonlinear vibration equation of the composite shaft-disk system. IHB method has the advantage of solving both small amplitude and large amplitude vibration problems. In particular, it is possible to solve the nonlinear structural vibration problems with periodic solutions, such as in the rotating shaft [21].

IHB method is a combination of harmonic balance method and incremental method, which is executed in two steps. The first is the incremental processing step of Newton–Raphson method. The independent time variable  $\tau$  is selected and assumed to be  $\tau = \Omega t$ , and this equation is replaced with Eq. (36) to obtain Eq. (38).

$$\Omega^2 \mathbf{m} \mathbf{p}'' + \Omega \mathbf{g}(\Omega) \mathbf{p}' + (\mathbf{k} + \mathbf{k}_3) \mathbf{p} = \Omega^2 \mathbf{f} \tag{38}$$



Suppose that the solution of Eq. (38) is a linear vibration solution corresponding to normal nonlinear vibration, and the next solution is obtained through the incremental process.

$$\Omega = \Omega_0 + \Delta\Omega \tag{39}$$

$$\mathbf{p} = \mathbf{p}_0 + \Delta\mathbf{p} \tag{40}$$

Substitute Eqs. (39) and (40) into Eq. (38) and ignore the higher-order quantities. Then the incremental variable equation can be obtained, as shown below.

$$\Omega\mathbf{m}\Delta\mathbf{p}'' + \Omega\mathbf{g}(\Omega)\Delta\mathbf{p}' + (\mathbf{k} + 3\mathbf{k}_3)\Delta\mathbf{p} = \mathbf{R} - (2\Omega\mathbf{m}\mathbf{p}_0'' + \mathbf{g}(\Omega)\mathbf{p}_0')\Delta\Omega \tag{41}$$

$$\mathbf{R} = \Omega^2\mathbf{f} - (\Omega^2\mathbf{m}\mathbf{p}_0'' + \Omega\mathbf{g}(\Omega)\mathbf{p}_0' + \mathbf{k}\mathbf{p}_0 + \mathbf{k}_3\mathbf{p}_0) \tag{42}$$

The second step is Ritz–Galerkin treatment for Eq. (41). The solution of Eq. (38) can be expressed as follows.

$$p_j = a_{j0} + \sum_{k=1}^n (a_{jk} \cos k\tau + b_{jk} \sin k\tau) = \mathbf{C}_s\mathbf{A}_j \tag{43}$$

$$\Delta p_j = \Delta a_{j0} + \sum_{k=1}^n (\Delta a_{jk} \cos k\tau + \Delta b_{jk} \sin k\tau) = \mathbf{C}_s\Delta\mathbf{A}_j \tag{44}$$

Here,

$$\mathbf{C}_s = [1 \quad \cos \tau \quad \cdots \quad \cos n\tau \quad \sin \tau \quad \cdots \quad \sin n\tau]^T \tag{45}$$

$$\mathbf{A}_j = [a_{j0} \quad a_{j1} \quad \cdots \quad a_{jn} \quad b_{j1} \quad \cdots \quad b_{jn}]^T \tag{46}$$

$$\Delta\mathbf{A}_j = [\Delta a_{j0} \quad \Delta a_{j1} \quad \cdots \quad \Delta a_{jn} \quad \Delta b_{j1} \quad \cdots \quad \Delta b_{jn}]^T \tag{47}$$

If  $\mathbf{p}_0$  and  $\Delta\mathbf{p}$  are expressed in vector format, it is as follows.

$$\mathbf{p}_0 = \mathbf{S}\mathbf{A}, \quad \Delta\mathbf{p} = \mathbf{S}\Delta\mathbf{A} \tag{48}$$

Here,

$$\begin{aligned} \mathbf{S} &= \text{diag}[\mathbf{C}_s \quad \mathbf{C}_s \quad \cdots \quad \mathbf{C}_s], \mathbf{A} \\ &= [\mathbf{A}_1 \quad \mathbf{A}_2 \quad \cdots \quad \mathbf{A}_N]^T, \Delta\mathbf{A} \\ &= [\Delta\mathbf{A}_1 \quad \Delta\mathbf{A}_2 \quad \cdots \quad \Delta\mathbf{A}_N]^T \end{aligned} \tag{49}$$

*diag* denotes a diagonal matrix and  $N$  denotes the total number of degrees of freedom. The total length of  $\mathbf{A}$  is  $len = N \times (2n + 1)$ . Replace Eq. (48) with Eq. (41) and proceed with Galerkin procedure.

$$\begin{aligned} &\int_0^{2\pi} \delta(\Delta\mathbf{p})^T [\Omega^2\mathbf{m}\Delta\mathbf{p}'' + \Omega\mathbf{g}(\Omega)\Delta\mathbf{p}' + (\mathbf{k} + 3\mathbf{k}_3)\Delta\mathbf{p}] d\tau \\ &= \int_0^{2\pi} \delta(\Delta\mathbf{p})^T [\mathbf{R} - (2\Omega\mathbf{m}\mathbf{p}_0'' + \Omega\mathbf{g}(\Omega)\mathbf{p}_0')\Delta\Omega] d\tau \end{aligned} \tag{50}$$

Equation (50) can be summarized as follows.

$$\bar{\mathbf{K}}_{mc}\Delta\mathbf{A} = \bar{\mathbf{R}} - \bar{\mathbf{R}}_{mc}\Delta\Omega \tag{51}$$

Here,

$$\bar{\mathbf{K}}_{mc} = \Omega^2\bar{\mathbf{M}} + \Omega\bar{\mathbf{G}}(\Omega) + \bar{\mathbf{K}} + 3\bar{\mathbf{K}}_3 \tag{52}$$

$$\bar{\mathbf{R}} = \bar{\mathbf{F}} - (\Omega^2\bar{\mathbf{M}} + \Omega\bar{\mathbf{G}}(\Omega) + \bar{\mathbf{K}} + \bar{\mathbf{K}}_3)\bar{\mathbf{A}} \tag{53}$$

$$\bar{\mathbf{R}}_{mc} = -[2\Omega\bar{\mathbf{M}} + \Omega\bar{\mathbf{G}}(\Omega)]\bar{\mathbf{A}} \tag{54}$$

$$\begin{aligned} \bar{\mathbf{M}} &= \int_0^{2\pi} \mathbf{S}^T \mathbf{m} \ddot{\mathbf{S}} d\tau \quad \bar{\mathbf{G}}(\Omega) = \int_0^{2\pi} \mathbf{S}^T \mathbf{g}(\Omega) \dot{\mathbf{S}} d\tau \\ \bar{\mathbf{K}} &= \int_0^{2\pi} \mathbf{S}^T \mathbf{k} \mathbf{S} d\tau \quad \bar{\mathbf{K}}_3 = \int_0^{2\pi} \mathbf{S}^T \mathbf{k}_3 \mathbf{S} d\tau \end{aligned} \tag{55}$$

$$\bar{\mathbf{F}} = \Omega^2 \int_0^{2\pi} \mathbf{S}^T \mathbf{f} d\tau$$

A detailed method for solving the nonlinear vibration problem using the IHB method is introduced in the reference [22].

### 6 Results and discussion

In order to prove the efficiency of the proposed method, the analytical results of the previous researches are compared with that calculated by the proposed method. Then, the linear and nonlinear vibration of shaft-disk system made of isotropic material is studied. Through the study of this model, the convergence process of the frequency–response characteristic curve with the increasing number of elements and integral points is investigated. Based on

this, the number of elements and integral points to be used in the analysis are determined. Besides, the number of modes to be applied in the reduced-order model is determined as well.

First, the proposed method is used to analyze the nonlinear forced vibration of the Jeffcott rotor, and the results are compared with the results of the previous literature. Saeed analyzed the nonlinear forced vibration of symmetric and asymmetric Jeffcott rotor system supported horizontally and vertically [23–26]. In this paper, the symmetric rotor system is analyzed, so it was compared with the analysis results of the nonlinear vibration of symmetric horizontally supported Jeffcott rotor published in [23]. Figure 3 shows the horizontally supported Jeffcott rotor system used in the analysis.

The motion equation of Jeffcott rotor is expressed with dimensionless parameters as follows.

$$\begin{aligned} \ddot{x}_1 + \mu_1 \dot{x}_1 + \omega_1^2 x_1 + 2\delta x_1 x_2 + \gamma(x_1^2 + x_2^2)x_1 \\ = f\Omega^2 \cos(\Omega t + \beta) \\ \ddot{x}_2 + \mu_2 \dot{x}_2 + \omega_2^2 x_2 + \delta(x_1^2 + 3x_2^2) + \gamma(x_1^3 + x_2^2)x_2 \\ = f\Omega^2 \sin(\Omega t + \beta) \end{aligned} \quad (56)$$

The calculative process of this formula is described in detail in the reference [23]. The frequency–response characteristic curves calculated by the method proposed are compared with the analysis results of the reference [23] as shown in Fig. 4. The displacement expression used when solving Eq. (56) by the IHB method is as follows

$$\begin{aligned} x_1 &= a_{11} + \sum_{k=1}^4 (a_{1k} \cos k\tau + b_{1k} \sin k\tau) \\ x_2 &= a_{21} + \sum_{k=1}^4 (a_{2k} \cos k\tau + b_{2k} \sin k\tau) \end{aligned} \quad (57)$$

The figure shows the frequency–response characteristics when the dimensionless variable  $f$  is 0.01, 0.015, 0.02, and 0.025. In the reference [23], the frequency–response curve was obtained from Eq. (56) using the multiple scales perturbation method. As shown in the figure, when  $f$  is small, it can be seen that the results calculated applying the previous method [23] and the proposed method are consistent. You can see that as  $f$  increases, there is a slight difference between the two results. In the figure, it can also be

seen that the results calculated using numerical integration (NI). All the solutions calculated using NI are stable [27]. Comparing the two results mentioned above with the results calculated by NI, it can be seen that the stable solutions are completely consistent regardless of the size of  $f$ .

Next, the linear and nonlinear vibrations of the shaft-disk system made of isotropic material are analyzed. The materials and geometric parameters used in the analysis are presented in Table 1.

The disk is mount at the 1/3 position of the total length. The eccentricity distribution of unbalanced mass  $e_\xi$  and  $e_\zeta$  distributed in the disk is all 0.001 m.

In the reference [28], the linear frequency–response characteristic curve according to the number of elements and integral points was studied. Therefore, only the convergence characteristic of the nonlinear frequency–response characteristic curve with the increase in the number of elements and integral points is presented here. Figure 5 shows the frequency response curves of the shaft-disk system according to the increase in the number of elements. Here, 5 integral points are fixed. As you can see in the figure, when the number of elements is 3, 6, and 9, the frequency–response characteristic curve is almost identical.

Figure 6 shows the frequency–response characteristic curves as the number of integral points increases. Here, the number of elements is fixed at 3. As can be seen in the figure, the number of integral points is 4, 5, 6. From Figs. 5 and 6, the number of elements is set to 3 and the number of integral points for each element is set to 5.

The reduced-order model is used to reduce the calculation time. When applying the reduced order model in the analysis, the number of modes must be reasonably determined to ensure the required computational precision without changing the properties of the system. Figure 7 shows the unbalanced response curves and Campbell diagrams as the number of modes increases.

Due to the gyroscopic moment, the shaft makes a whirling motion and the natural frequency is changed according to the rotating speed. At this time, the whirling motion in the same direction with the shaft rotation is called forward whirl and that in the reverse direction is called back whirl (BW). When the shaft is rotating, the major critical speed is determined by the

**Table 1** Material and geometric parameters of shaft and disk

$E$ (Mpa)	$\rho$ (kg/m <sup>3</sup> )	$\mu$	$L$ (m)	$R_1$ (m)	$R_2$ (m)	$h$ (m)
2e11	7800	0.3	0.9	0.01	0.15	0.03

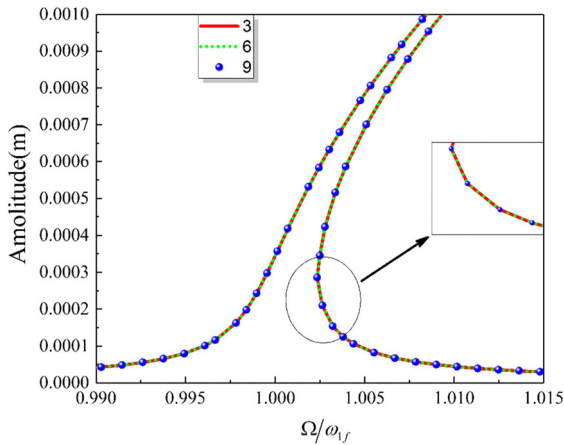


**Fig. 5** Frequency–response characteristic curve with the increase in the number of elements

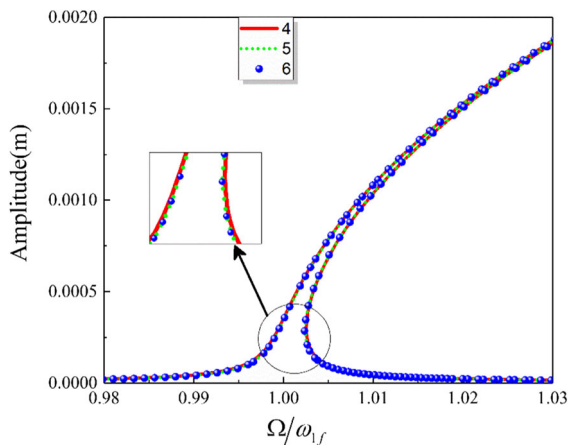


**Fig. 6** Frequency–response characteristic curve with the increase of integral points

cross points between the lines  $F = N/60$ ,  $FW$  and  $BW$ . Here,  $N$  indicates the rotation speed (rpm).

As can be seen in the figures, the results are all very similar in all cases. Among them, third and fourth cases are more similar.

Figure 8 shows the nonlinear vibration characteristic of rotor system calculated by adding the geometric nonlinearity of shaft into the linear analysis calculated above. The analysis is conducted at around the first frequency. Figures 7 and 8 show that, in the linear and nonlinear vibration calculation, the reduced-order method not only reduces the calculation time greatly, but also the sufficient calculation precision can be obtained. The nonlinear vibration characteristics are analyzed using four modes in total, that is, from mode number 1 to 4. The total degree of freedom in the non-reduced-order model is 65, while it is 8 in the reduced-order model. Although the significance of mode-reduction is not considerable in the linear vibration calculation, it is very obvious in the nonlinear vibration calculation in which the solution is obtained through the repeated calculation, which means the amount of time is much reduced if the nonlinear vibration characteristics are calculated using the reduced-order model.

The nonlinear vibration characteristics of the composite shaft mounted with a disk are analyzed using the proposed method. In reference [14], the nonlinear vibration of the composite shaft mounted with disk was analyzed and the frequency–response curve according to the change of the various parameters was obtained. In this article, the nonlinear vibration phenomenon of the composite shaft-disk system occurred at different rotating speeds is studied. The material and geometric properties of shaft used in the analysis are given in Table 2.

The disks are mounted at the 1/3, 2/3 positions of total length. The external radii of the first and second steel disk are 0.15 m and 0.2 m, respectively, and their thickness are all 0.005 m. The eccentricity distribution of unbalanced mass  $e_x$  and  $e_z$  distributed in the disk is all 0.001 m. The composite shaft consists of 8 layers and the stacking sequence is  $[90_2, 45, 0]_s$ .

First, it is checked whether the internal resonance could occur by conducting the analysis of linear vibration analysis of the composite shaft-disk system.

**Fig. 7** Comparison of linear vibration analysis using the reduced and non-reduced order model

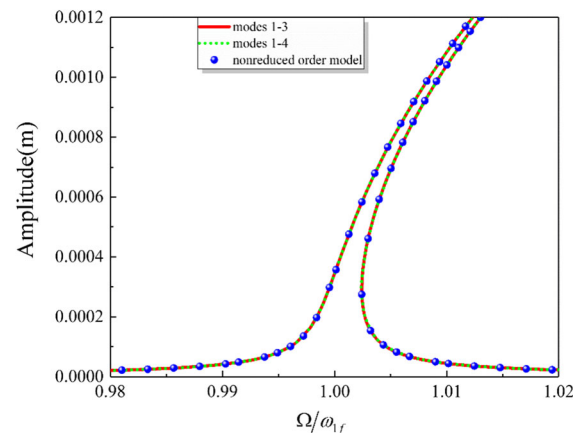
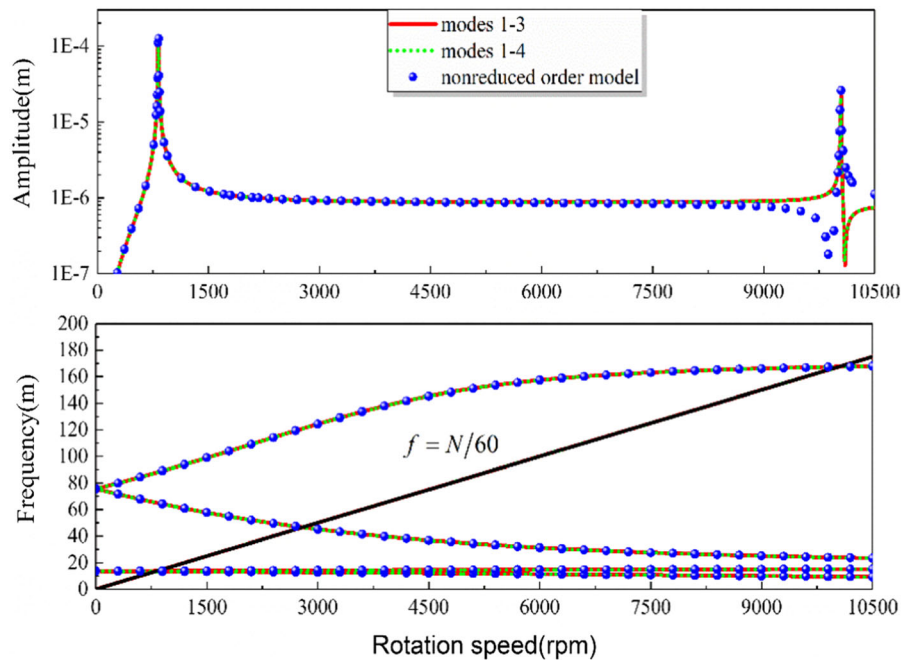


**Fig. 8** Comparison of nonlinear vibration analysis using the reduced and non-reduced order model

Figure 9 shows the unbalanced response and Campbell diagram of the composite shaft-disk system with the properties of Table 2. All the quantities marked on the figure are non-dimensional. In this article, only the

relationship between the critical speeds in the forward direction is considered. In the forward direction, the first critical speed is 0.1614 and the second critical speed is 0.5352, that is,  $0.5352/0.1614 \approx 3.3$ ; therefore, there are possibilities that the internal resonance can occur between the first and second modes. Based on these considerations, the characteristics of nonlinear vibration occurred at several rotating speeds are studied.

The nonlinear vibration phenomenon occurred near the first natural frequency is considered. The frequency–response curve shown in Figs. 5 and 6 is the most general form. In reality, the shape of frequency–response curve occurred at several resonance points is not so simple if the internal resonance exists. Figure 10 shows the frequency–response of composite shaft-disk system occurred when the external excitation frequency is near the first critical speed.

The displacement expression applied in Fig. 10 is as follows.

**Table 2** Material and geometric properties of shaft

$E_1$ (GPa)	$E_2$ (GPa)	$G_{12}$ (GPa)	$\mu_{12}$	$\rho_s$ (Kg/m <sup>3</sup> )	$L$ (m)	$H$ (m)	$R_1$ (m)
172	7.2	3.76	0.3	1446.2	1.2	0.008	0.048

**Fig. 9** Unbalanced response and Campbell diagram of the composite shaft-disk system

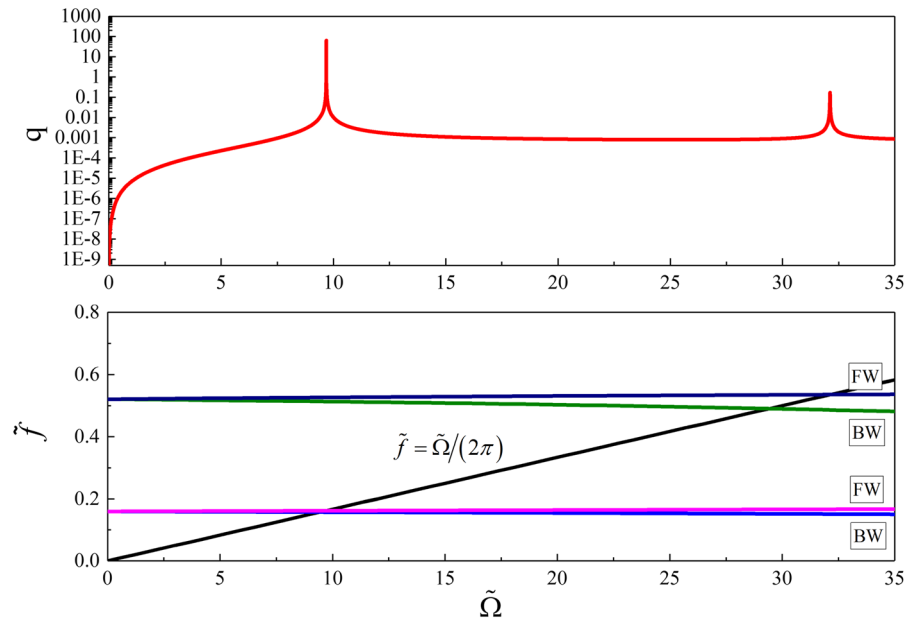
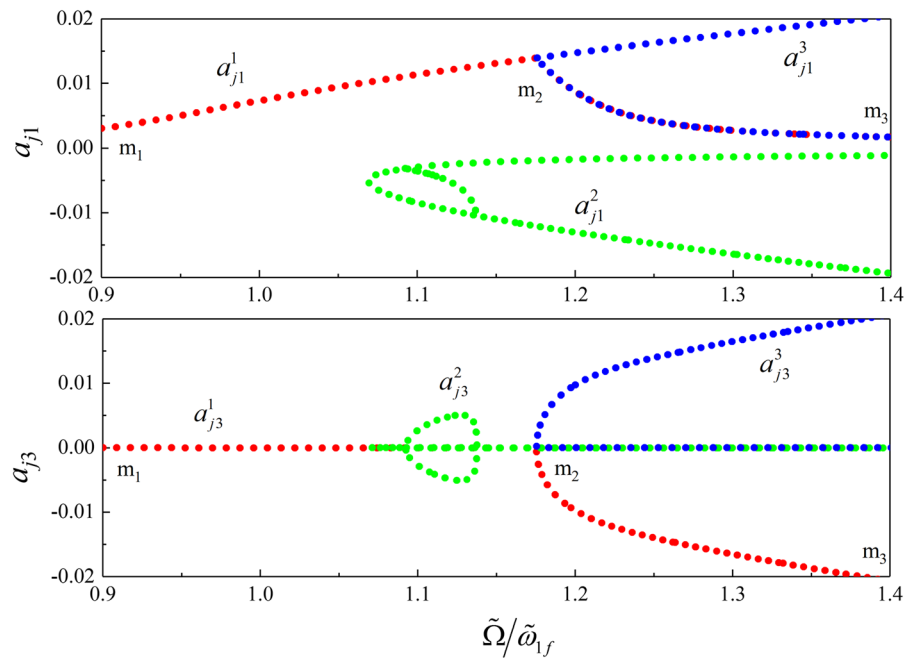


**Fig. 10** Frequency–response curve of the composite shaft-disk system near the first critical speed



$$p_j = a_{j1} \cos \tau + a_{j3} \cos 3\tau + \dots + b_{j1} \sin \tau + b_{j3} \sin 3\tau + \dots$$

$$\Delta a_{j1} \cos \tau + \Delta a_{j3} \cos 3\tau + \dots + \Delta b_{j1} \sin \tau + \Delta b_{j3} \sin 3\tau + \dots \quad (58)$$

As can be seen in figure, there are three solution branches in this section. The first branch starts at  $m_1$  and the transfer of energy takes place between the first

and second items of harmonic terms at  $m_2$ , that is,  $|a_{j1}| > |a_{j3}|$  from  $m_1$  to  $m_2$  while  $|a_{j1}| < |a_{j3}|$  from  $m_2$  to  $m_3$ . There are several vibration modes on the elastic object. In the linear vibration system, among these modes, only the modes with same frequency as the external excitation force are excited and rest of non-excited modes are static, that is, modes are

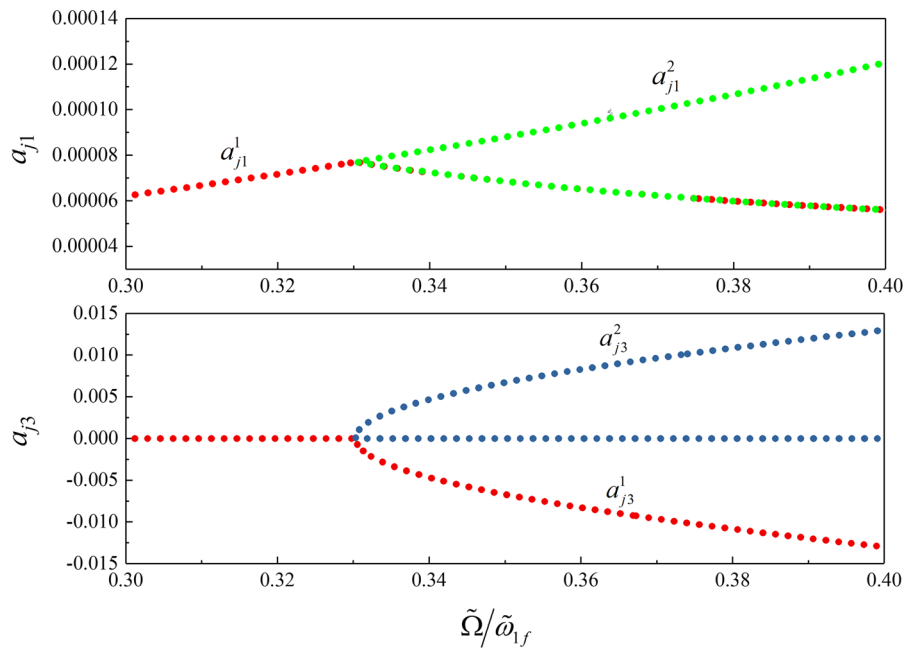
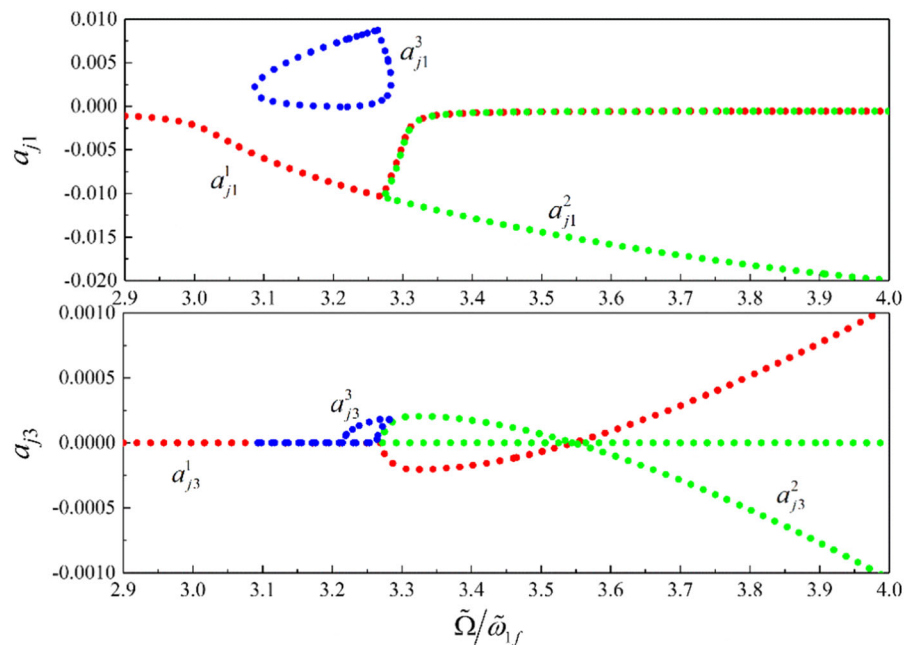


**Fig. 11** Frequency–response curve at about 1/3 of the first critical speed

**Fig. 12** Frequency–response curve of the composite shaft–disk system near the second critical speed (fundamental resonance)

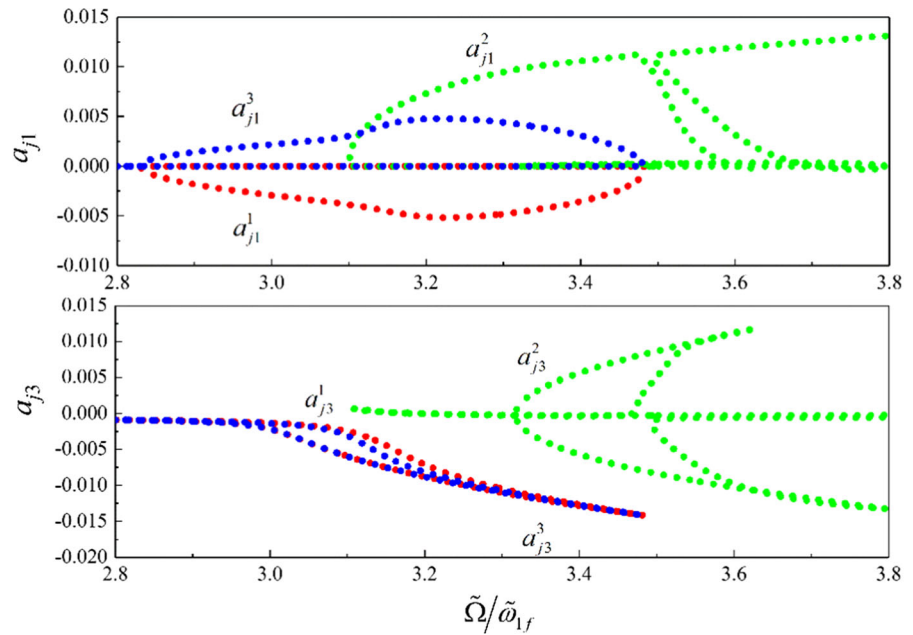


independent each other. However, in the nonlinear vibration, different modes are combined each other to response to the external excitation force. In other word, if any mode related with the frequency of external excitation force is excited, the energy is transferred to other modes, exciting them. Therefore,

the third harmonic term ( $\cos 3\tau$ ) is excited not because of the external excitation force, but because of the nonlinearity of system. This phenomenon is called internal resonance.

Figure 11 shows the frequency–response curve at about 1/3 of the first critical speed. Equation (58) is

**Fig. 13** Frequency–response curves of the composite shaft-disk system near the second critical speed (sub-harmonic resonance)



also used in the displacement expression. The figure shows that the coefficient of the third harmonic term ( $\cos 3\tau$ ) is the largest. The coefficients of other harmonic terms are very small compared to this term and hence are not shown. This means that resonance occurs at the frequency three times the external excitation frequency. This resonance is called super-harmonic resonance.

Figures 12 and 13 show the frequency–response curves when the external excitation frequency is three times of the first critical speed, that is, near the second critical speed. When the external excitation frequency is near this frequency, the fundamental resonance and sub-harmonic resonance take place. Figure 12 shows the frequency–response curve of the fundamental resonance occurred when the external excitation frequency is near the second critical speed.

Equation (58) is used in the displacement expression for calculating the fundamental resonance. The displacement expression used in the calculation of sub-harmonic resonance is as follows.

$$\begin{aligned}
 p_j &= a_{j1} \cos \tau/3 + a_{j3} \cos \tau + \dots b_{j1} \sin \tau/3 + b_{j3} \sin \tau + \dots \\
 \Delta p_j &= \Delta a_{j1} \cos \tau/3 + \Delta a_{j3} \cos \tau + \dots \Delta b_{j1} \sin \tau/3 + \Delta b_{j3} \sin \tau + \dots
 \end{aligned}
 \tag{59}$$

Figure 13 shows the frequency–response curve of the sub-harmonic resonance occurred when the

external excitation frequency is near the second critical speed. As can be seen in the figure, the coefficients of harmonic term have very complex forms in all the solution branches. This is because that the internal resonance phenomenon is appeared between two modes as the ratio of first critical speed and second critical speed is about 1:3. This internal resonance has more complex forms than that occurred at other critical speeds.

### 7 Conclusion

In this paper, the nonlinear forced vibration of the composite shaft-disk system caused by the unbalanced mass is analyzed. The stiffness coefficients are calculated using the SHBT; the element matrix is established using the WQEM. Lagrange’s equation is used to construct the motion equation while the FEM is applied to calculate the system matrix. To reduce the calculation time, the reduced-order model is used and the nonlinear equation is solved by the IHB method. The effectiveness of the proposed model is validated through the analysis of the nonlinear forced vibration of Jeffcott rotor and the model is extended into the multi-degrees of freedom model, based on which the method for solving the nonlinear vibration equation is established. Using the proposed method, the

frequency–response curve appeared at several resonance points is constructed. This paper has not reported the analysis on the stability of the solution, which will be proposed in the next paper.

**Declaration**

**Conflict of interest** The authors declare that they have no conflict of interest.

**Appendix**

The every element matrix in Eq. (31) is expressed as follows.

The mass matrix is as follows.

$$\mathbf{M}^e = \mathbf{M}_d^e + \mathbf{M}_s^e \tag{60}$$

Here,  $\mathbf{M}_d^e$  is the mass matrix of the disk and expressed as follows.

$$\mathbf{G}^e = \mathbf{G}_d^e + \mathbf{G}_s^e \tag{63}$$

Here,  $\mathbf{G}_d^e$  is the gyroscopic matrix of the disk and expressed as follows.

$$\mathbf{G}_d^e = \begin{bmatrix} 0 & 0 & 0 & 0 & 0 \\ 0 & 0 & 0 & 0 & 0 \\ 0 & 0 & 0 & 0 & 0 \\ 0 & 0 & 0 & 0 & -\tilde{I}_{dpi} \\ 0 & 0 & 0 & \tilde{I}_{dpi} & 0 \end{bmatrix} \tag{64}$$

$\mathbf{G}_s^e$  is the gyroscopic matrix of shaft element and expressed as follows.

$$\mathbf{G}_s^e = \begin{bmatrix} \mathbf{0} & \mathbf{0} & \mathbf{0} & \mathbf{0} & \mathbf{0} \\ \mathbf{0} & \mathbf{0} & \mathbf{0} & \mathbf{0} & \mathbf{0} \\ \mathbf{0} & \mathbf{0} & \mathbf{0} & \mathbf{0} & \mathbf{0} \\ \mathbf{0} & \mathbf{0} & \mathbf{0} & \mathbf{0} & -\tilde{I}_2 \mathbf{C}^{(1)} \\ \mathbf{0} & \mathbf{0} & \mathbf{0} & \tilde{I}_2 \mathbf{C}^{(1)} & \mathbf{0} \end{bmatrix} \tag{65}$$

The stiffness matrix of shaft element is as follows.

$$\mathbf{K}_s^e = \begin{bmatrix} \tilde{E}_{eqs} \mathbf{A}^{(1)T} \mathbf{C}^{(1)} \mathbf{A}^{(1)} & \mathbf{0} & \mathbf{0} & \mathbf{0} & \mathbf{0} \\ \mathbf{0} & \tilde{G}_{eq} \mathbf{A}^{(1)T} \mathbf{C}^{(1)} \mathbf{A}^{(1)} & \mathbf{0} & \mathbf{0} & -\tilde{G}_{eq} \mathbf{A}^{(1)T} \mathbf{C}^{(1)} \mathbf{I} \\ \mathbf{0} & \mathbf{0} & \tilde{G}_{eq} \mathbf{A}^{(1)T} \mathbf{C}^{(1)} \mathbf{A}^{(1)} & \tilde{G}_{eq} \mathbf{A}^{(1)T} \mathbf{C}^{(1)} \mathbf{I} & \mathbf{0} \\ \mathbf{0} & \mathbf{0} & \tilde{G}_{eq} \mathbf{I}^T \mathbf{C}^{(1)} \mathbf{A}^{(1)} & \tilde{E}_{eq} \mathbf{A}^{(1)T} \mathbf{C}^{(1)} \mathbf{A}^{(1)} & \mathbf{0} \\ \mathbf{0} & -\tilde{G}_{eq} \mathbf{I}^T \mathbf{C}^{(1)} \mathbf{A}^{(1)} & \mathbf{0} & \mathbf{0} & \tilde{E}_{eq} \mathbf{A}^{(1)T} \mathbf{C}^{(1)} \mathbf{A}^{(1)} \end{bmatrix} \tag{66}$$

$$\mathbf{M}_d^e = \begin{bmatrix} \tilde{M}_{di} & 0 & 0 & 0 & 0 \\ 0 & \tilde{M}_{di} & 0 & 0 & 0 \\ 0 & 0 & \tilde{M}_{di} & 0 & 0 \\ 0 & 0 & 0 & \tilde{I}_{di} & 0 \\ 0 & 0 & 0 & 0 & \tilde{I}_{di} \end{bmatrix} \tag{61}$$

$\mathbf{M}_s^e$  is the mass matrix of shaft element and expressed as follows.

$$\mathbf{M}_s^e = \begin{bmatrix} \mathbf{C}^{(1)} & 0 & 0 & 0 & 0 \\ 0 & \mathbf{C}^{(1)} & 0 & 0 & 0 \\ 0 & 0 & \mathbf{C}^{(1)} & 0 & 0 \\ 0 & 0 & 0 & \tilde{I}_1 \mathbf{C}^{(1)} & 0 \\ 0 & 0 & 0 & 0 & \tilde{I}_1 \mathbf{C}^{(1)} \end{bmatrix} \tag{62}$$

The gyroscopic matrix is as follows.

The nonlinear stiffness matrix of shaft element is as follows.



$$\mathbf{K}_3^e = \frac{\tilde{E}_{eqs}}{2} \begin{bmatrix}
 \mathbf{0} & \psi \mathbf{A}^{(1)T} \mathbf{C}^{(1)} \left( \mathbf{A}^{(1)} \boldsymbol{\nu} \right) \mathbf{A}^{(1)} & \psi \mathbf{A}^{(1)T} \mathbf{C}^{(1)} \left( \mathbf{A}^{(1)} \boldsymbol{w} \right) \mathbf{A}^{(1)} & \mathbf{0} & \mathbf{0} \\
 2\psi \mathbf{A}^{(1)T} \mathbf{C}^{(1)} \left( \mathbf{A}^{(1)} \boldsymbol{\nu} \right) \mathbf{A}^{(1)} & \psi^2 \mathbf{A}^{(1)T} \mathbf{C}^{(1)} \left( \mathbf{A}^{(1)} \boldsymbol{\nu} \right)^2 \mathbf{A}^{(1)} & \psi^2 \mathbf{A}^{(1)T} \mathbf{C}^{(1)} \left( \mathbf{A}^{(1)} \boldsymbol{\nu} \right) \left( \mathbf{A}^{(1)} \boldsymbol{w} \right) \mathbf{A}^{(1)} & \mathbf{0} & \mathbf{0} \\
 2\psi \mathbf{A}^{(1)T} \mathbf{C}^{(1)} \left( \mathbf{A}^{(1)} \boldsymbol{\nu} \right) \mathbf{A}^{(1)} & \psi^2 \mathbf{A}^{(1)T} \mathbf{C}^{(1)} \left( \mathbf{A}^{(1)} \boldsymbol{w} \right) \left( \mathbf{A}^{(1)} \boldsymbol{\nu} \right) \mathbf{A}^{(1)} & \psi^2 \mathbf{A}^{(1)T} \mathbf{C}^{(1)} \left( \mathbf{A}^{(1)} \boldsymbol{w} \right)^2 \mathbf{A}^{(1)} & \mathbf{0} & \mathbf{0} \\
 \mathbf{0} & \mathbf{0} & \mathbf{0} & \mathbf{0} & \mathbf{0} \\
 \mathbf{0} & \mathbf{0} & \mathbf{0} & \mathbf{0} & \mathbf{0}
 \end{bmatrix} \tag{67}$$

Here,  $\mathbf{0}$  and  $\mathbf{I}$  are zero matrix and identity matrix, respectively.

**References**

1. Benamar, R., Bennouna, M.M.K.: The effects of large vibration amplitudes on the mode shapes and natural frequencies of thin elastic structures part I: simply supported and clamped-clamped beams. *J. Sound Vib.* **149**(2), 179–195 (1991)
2. Singh, S.P., Gupta, K.: Dynamic analysis of composite rotors. *Int. J. Rotating Mach.* **2**(3), 179–186 (1996)
3. Gubran, H.B.H., Gupta, K.: The effect of stacking sequence and coupling mechanisms on the natural frequencies of composite shafts. *J. Sound Vib.* **282**, 231–248 (2005)
4. Sino, R., Baranger, T.N., Chatelet, E., Jacquet, G.: Dynamic analysis of a rotating composite shaft. *Compos. Sci. Technol.* **68**, 337–345 (2008)
5. Ri, K., Choe, K., Han, P., Wang, Q.: The effects of coupling mechanisms on the dynamic analysis of composite shaft. *Compos. Struct.* **224**, 111040 (2019)
6. Singh, S.P., Gupta, K.: Composite shaft rotordynamic analysis using a layerwise theory. *J. Sound Vib.* **191**(5), 739–756 (1996)
7. Ishida, Y., Nagasaka, I., Inoue, T., Lee, S.: Forced oscillations of a vertical continuous rotor with geometric nonlinearity. *Nonlinear Dyn.* **11**, 107–120 (1996)
8. Ishida, Y., Inoue, T.: Internal resonance phenomena of the Jeffcott rotor with nonlinear spring characteristics. *ASME* **126**, 476–484 (2004)
9. Ishida, Y., Inoue, T.: Internal resonance phenomena of an asymmetrical rotating shaft. *J. Vib. Control* **11**(9), 1173–1193 (2005)
10. Inoue, T., Ishida, Y.: Chaotic vibration and internal resonance phenomena in rotor systems. *ASME* **128**, 156–169 (2006)
11. Khadem, S.E., Shahgholi, M., Hosseini, S.A.A.: Primary resonances of a nonlinear in-extensional rotating shaft. *Mech. Mach. Theory* **45**, 1067–1081 (2010)
12. Hosseini, S.A.A., Zamanian, M.: Multiple scales solution for free vibrations of a rotating shaft with stretching nonlinearity. *Sci Iran* **20**(1), 131–140 (2013)
13. Hosseini, S.A.A., Zamanian, M., Shams, Sh., Shooshtari, A.: Vibration analysis of geometrically nonlinear spinning beams. *Mech. Mach. Theory* **78**, 15–35 (2014)
14. Zhang, C., Ren, Y., Ji, S.: Research on lateral nonlinear vibration behavior of composite shaft-disk rotor system. *Appl. Mech. Mater.* **875**, 149–161 (2018)
15. Nezhad, H.S.A., Hosseini, S.A.A., Tiaki, M.M.: Combination resonances of spinning composite shafts considering geometric nonlinearity. *J. Braz. Soc. Mech. Sci.* **41**(11), 515 (2019)
16. Shaban, A.N.H., Hosseini, S.A.A.: Flexural–flexural–extensional–torsional vibration analysis of composite spinning shafts with geometrical nonlinearity. *Nonlinear Dyn.* **89**, 651–690 (2017)
17. Saeed, N.A.: On vibration behavior and motion bifurcation of a nonlinear asymmetric rotating shaft. *Arch. Appl. Mech.* **89**(9), 1899–1921 (2019)
18. Wang, X., Yuan, Z., Jin, C.: Weak form quadrature element method and its applications in science and engineering: a state-of-the-art review. *Appl. Mech. Rev.* **69**, 030801 (2017)
19. Ahmad, M., Mohammad, H.K.: Nonlinear dynamic analysis of an axially loaded rotating timoshenko beam with extensional condition included subjected to general type of force moving along the beam length. *J. Vib. Control* **19**(16), 2448–2458 (2012)
20. Lalanne, M., Ferraris, G.: *Rotordynamics Prediction in Engineering*. Wiley, New York (1998)
21. Cheung, Y.K., Chen, S.H., Lau, S.L.: Application of the incremental harmonic balance method to cubic non-linearity systems. *J. Sound Vib.* **140**(2), 273–286 (1990)
22. Ri, K., Han, P., Kim, I., Kim, W., Cha, H.: Nonlinear forced vibration analysis of composite beam combined with DQFEM and IHB. *AIP Adv.* **10**, 885112 (2020)
23. Saeed, N.A.: On the steady-state forward and backward whirling motion of asymmetric nonlinear rotor system. *Eur. J. Mech. A-solid.* **80**, 103878 (2019)
24. Saeed, N.A., Awwad, E.M., El-Meligy, M.A., Nasr, E.A.: Sensitivity analysis and vibration control of asymmetric nonlinear rotating shaft system utilizing 4-pole AMBs as an actuator. *Eur. J. Mech. A-solid.* **86**, 104145 (2020)
25. Saeed, N.A., Eissa, M.: Bifurcation Analysis of a Transversely Cracked Nonlinear Jeffcott Rotor System at Different Resonance Cases. *Int. J. Acoust. Vib.* **24**(2), 284–302 (2019)
26. Eissa, M., Kamel, M., Saeed, N.A., El-Ganaini, W.A., El-Gohary, H.A.: Time-delayed positive-position and velocity feedback controller to suppress the lateral vibrations in

- nonlinear Jeffcott-rotor system. *Minufiya J. of Electronic Engineering Research* **27**(1), 1–16 (2017)
27. Krack, M., Gross, J.: *Harmonic Balance for Nonlinear Vibration Problems*. Springer (2019)
28. Ri, K., Han, P., Kim, I., Kim, W., Cha, H.: Stability analysis of composite shafts considering internal damping and coupling Effect. *Int. J. Struct. Stab. Dyn.* **20**(11), 1–25 (2020)

**Publisher's Note** Springer Nature remains neutral with regard to jurisdictional claims in published maps and institutional affiliations.